Check for updates

Robust Negative Electrode Materials Derived from Carbon Dots and Porous Hydrogels for High-Performance Hybrid Supercapacitors

Ji-Shi Wei, Chen Ding, Peng Zhang, Hui Ding, Xiao-Qing Niu, Yuan-Yuan Ma, Chao Li, Yong-Gang Wang, and Huan-Ming Xiong**

Hybrid supercapacitors generally show high power and long life spans but inferior energy densities, which are mainly caused by carbon negative electrodes with low specific capacitances. To improve the energy densities, the traditional methods include optimizing pore structures and modifying pseudocapacitive groups on the carbon materials. Here, another promising way is suggested, which has no adverse effects to the carbon materials, that is, constructing electron-rich regions on the electrode surfaces for absorbing cations as much as possible. For this aim, a series of hierarchical porous carbon materials are produced by calcinating carbon dots–hydrogel composites, which have controllable surface states including electron-rich regions. The optimal sample is employed as the negative electrode to fabricate hybrid supercapacitors, which show remarkable specific energy densities (up to 62.8–90.1 Wh kg^{-1}) in different systems.

Hybrid supercapacitors (or hybrid batteries), composed of a battery-type electrode and a capacitive carbon-based electrode, are attracting extensive attention recently, because they combine high energy density of batteries and both high power density and long life span of supercapacitors.[1–7] Over the past years, many hybrid supercapacitors have been developed on the basis of activated carbon (AC), such as $Ni(OH)_2$//AC,[8] NiO_x//AC,[9] CoO_x//AC,[6] MnO_2//AC,[10,11] $LiMn_2O_4$//AC,[12] PbO_2//AC,[13] etc. The energy densities of these devices are higher than those of the traditional supercapacitors, but still lower than those of the conventional batteries (the disparities are about 5–10 times).[8,14–18] The problem is that the specific capacitances of common carbon negative electrodes are only 100–400 F g^{-1}, amounting to 10–30% of the positive electrodes' capacitances.[8,14,17,18] When fabricating hybrid supercapacitors, 3–5 folds or more amounts of carbon materials are required to fill the capacitance gap between the positive/negative electrodes, which finally restrict the whole energy densities of the devices. To improve electrochemical capacitances of carbon materials, three main strategies have been investigated thoroughly: enlarging specific surface areas,[19] constructing porous structures,[20,21] and introducing pseudocapacitive reactions.[22] But each strategy is not perfect. When the surface areas and the pore volumes are improved, the tap densities of electrodes will be reduced. Moreover, enhancing pseudocapacitance by modifying too many functional groups will decrease the whole conductivity and stability of electrode materials.[23]

In the present work, we suggest a new concept of building electron-rich regions on the electrode surface, so as to adsorb more cations and accelerate the charge transfer. As a result, the capacitance of carbon materials will be increased reasonably without sacrificing the density, conductivity, and stability of the whole electrode. However, this idea brings a new challenge because the desired groups with abundant electrons (like phosphate groups) are usually difficult to be modified on the carbon materials. In order to resolve this problem, we used carbon dots (CDs, sub-10 nm)[24,25] with desired groups as the guest, and the commercial polyacrylamide (PAM) hydrogel as the host. After calcination on the host–guest composites, we obtained new carbon frameworks which have abundant electron-rich regions, large surface areas, and appropriate porous structures in the meantime. The optimal sample exhibits a specific capacitance up to 468, 510, and 438 F g^{-1} in alkaline, acidic, and neutral electrolytes, respectively. When it is fabricated into a hybrid supercapacitors with the positive electrode material $Ni(OH)_2$/CNTs using an alkaline electrolyte, the mass ratio of positive/negative electrodes is less than 2, an energy density over 90 Wh kg^{-1} is realized successfully, and 100% of capacity retention rate is recorded after 10 000 cycles. This material also shows excellent performances in both acidic (PbO_2 as positive electrode) and neutral ($LiMn_2O_4$ as positive electrode) systems. Detailed structural characterizations and theoretical calculations prove that the well-preserved phosphate/nitrogen groups from the CDs precursors can effectively modulate the electronic structure and form electron-rich regions on the electrode

---

Dr. J.-S. Wei, Dr. C. Ding, Dr. P. Zhang, Dr. H. Ding, Dr. X.-Q. Niu,
Dr. Y.-Y. Ma, Dr. C. Li, Prof. Y.-G. Wang, Prof. H.-M. Xiong
Department of Chemistry
Shanghai Key Laboratory of Molecular Catalysis and Innovative Materials
Laboratory of Advanced Materials
Fudan University
Shanghai 200438, P. R. China
E-mail: ygwang@fudan.edu.cn; hmxiong@fudan.edu.cn

The ORCID identification number(s) for the author(s) of this article can be found under https://doi.org/10.1002/adma.201806197.

DOI: 10.1002/adma.201806197

© 2018 WILEY-VCH Verlag GmbH & Co. KGaA, Weinheim

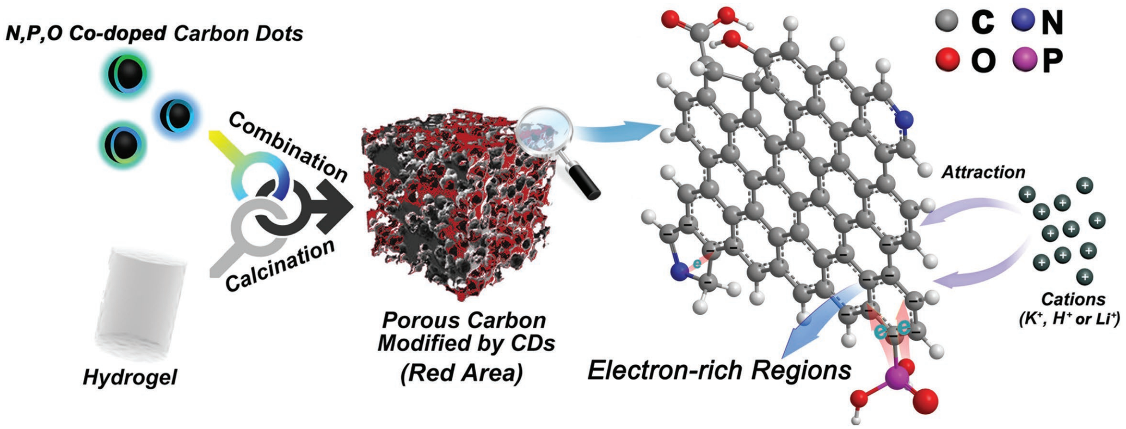

Scheme 1. The porous carbon is derived from carbon dots and PAM hydrogels. This material has plenty of functional groups and electron-rich defects for cations adsorption/reaction.

surfaces to adsorb plenty of cations. In comparison with those reported carbon materials for hybrid supercapacitors, our CDs–hydrogels derived materials exhibit great advantages in its controllable surface compositions and physical structures which can be both predicted theoretically and realized experimentally.

Scheme 1 illustrates the fabrication route of our porous carbon material from CDs and hydrogel. The porous PAM gel with 3D-interconnected networks was immersed into a NaCl/$ZnCl_2$ aqueous solution and a CDs aqueous solution, respectively, and then annealed in N_2 atmosphere to produce the hierarchical porous carbon (HPC) materials. After detailed characterizations and balanced evaluations, we found that the HPC derived from the CDs co-doped by phosphorus, nitrogen, and oxygen elements (NPOCD/HPC) had the best structure, which involved its pore size distribution, surface element composition, and charge distribution. For comparison, we used the CDs-free PAM hydrogel to prepare Free-HPC as control under the same condition.

The nitrogen adsorption–desorption isotherms of the Free-HPC and the NPOCDs/HPC are compared in **Figure 1**A (inset), which shows H4 type hysteresis loops at relative pressure of 0.3–1.0, implying that these porous materials composed of slit like hierarchical pores and micropores are dominant. The corresponding pore size distribution curves based on density functional theory (DFT) method display that the pore diameters focus on 0.7–0.8 and 1–2 nm, which fit for the hydrated K^+ and H^+ ions perfectly.[26–28] It also has pore size in the range of 2.3–4.0 nm, so that ions can transport freely along the channels.

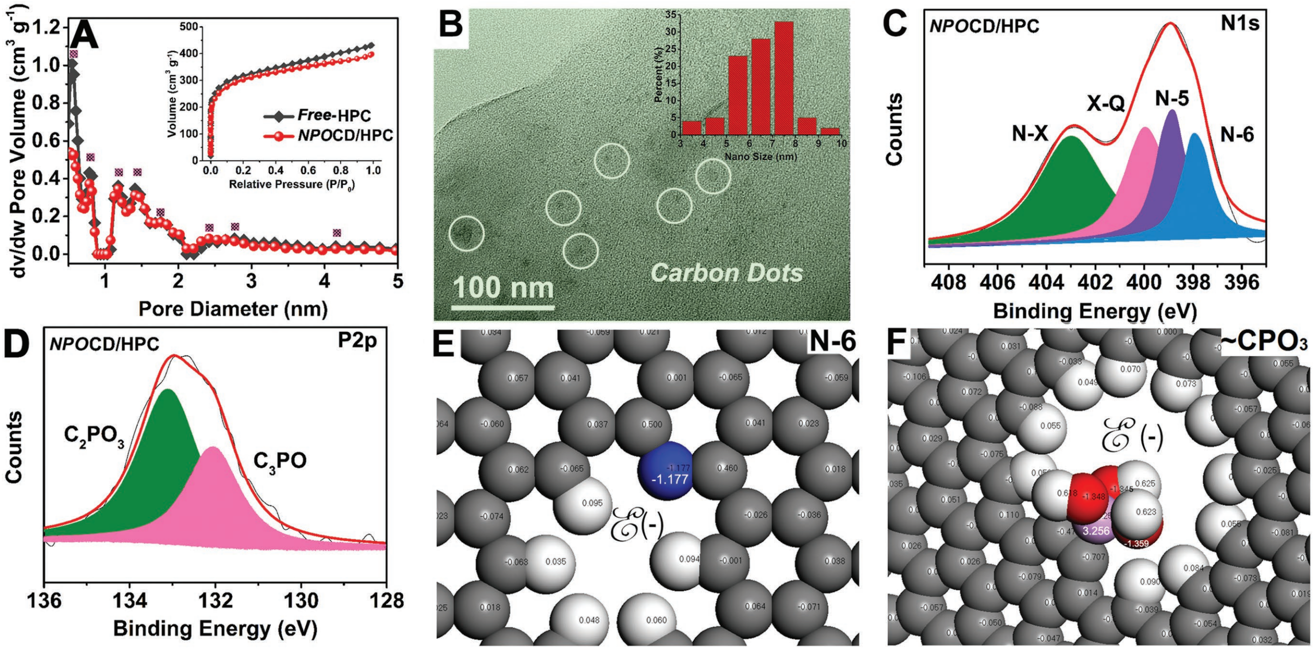

Figure 1. A) Pore size distributions calculated by the DFT method, and nitrogen adsorption–desorption isotherms (inset). B) For NPOCD/HPC, FETEM images (high magnification) and size distribution of carbon dots (inset). C,D) High-resolution XPS of N 1s and P 2p. E,F) DFT calculations of the charge distributions of nitrogen (N-6) and phosphorus (~CPO_3) doped functional groups.

© 2018 WILEY-VCH Verlag GmbH & Co. KGaA, Weinheim

Besides, Table S1 in the Supporting Information and Figure S5 in the Supporting Information show that the specific surface areas and pore volumes of two samples have similar structural properties. Therefore, CDs incorporation has little influence on the structures of hydrogel networks, as well as the final porous properties of HPC. Through high-resolution transmission electron microscopy (HRTEM) images of the optimal sample (Figure 1B and Figure S6, Supporting Information), CDs can be found on the carbon skeleton, whose sizes are mainly distributed from 5 to 8 nm. SEM images (Figure S7, Supporting Information) show all HPC samples have sponge-like nanoblocks with similar mesopores and micropores, in accordance with the above analyses.

Since the energy storage mainly depends on the interfacial reactions in a supercapacitor, the surface groups of electrode materials are important for interpreting their performances.[29–31] All HPC samples have graphitized skeletons as indicated by their X-ray diffraction patterns (Figure S8A, Supporting Information), and also by the presence of many active groups like P=O/P—O and C—N derived from CDs (see FTIR spectra in Figure S8B in the Supporting Information). The high-resolution X-ray photoelectron spectroscopy (XPS) analyses (Figure 1C,D, Figure S9, and Tables S2 and S3, Supporting Information) further confirm that both CDs precursors and the CDs/HPC products have plenty of various functional groups. Particularly for NPOCDs, the heteroatoms content is even over 30 wt% (Table S3, Supporting Information). It is clear that the P contents in CDs precursors are preserved effectively by our soaking–calcination method. For example, the P contents in NPOCDs and NPOCD/HPC are 5.23 and 1.99 wt%, respectively. Since the mass ratio of CDs and PAM gel is 1:1 before calcination, the P retention rate is over 76% from the precursors to the final products. In contrast, when phytic acid is employed to introduce P element into PAM gel instead of CDs, the final N, P, O co-doped HPC has only 1.01 wt% of P and the corresponding retention rate is only 38% (Table S3, Supporting Information). Therefore, employing CDs precursors is very effective to adjust the final surface states of CDs/HPC (Figure S10, Supporting Information). Furthermore, the water contact angle measurements (Figure S11, Supporting Information) illustrate that CDs incorporation significantly improve the wettability of HPC. The optimal NPOCD/HPC shows a contact angle of 8.9°, much smaller than that of the Free-HPC (17.1°).

DFT calculations on the charge distributions of surface groups are conducted to study the influences of functional groups on the electronic and microstructural properties of HPC.[32–34] In order to facilitate the comparison, charge distributions of different functional groups from NPOCD/HPC are picked, which has the most diverse functional groups. As shown in Figure 1E,F and Figure S12 in the Supporting Information, some specific groups like pyridine-type nitrogen (N-6), phosphate group ($-CPO_3$) or carboxyl (—COOH) can generate a significant charge change in the surrounding carbon atoms (e.g., from –0.013 to –0.707), while such influence from other groups including oxidized nitrogen (N-X) or quaternary nitrogen (N-Q) are relatively limited (e.g., from –0.005 to –0.041). Such powerful results confirm that these specific groups are not solely effective electron donors. They can also promote charge changes of the surrounding atoms so as to form large clusters of electron donors. When these electron donors combine with electron acceptors (cations) directly, a great capacitance with a high rate in dynamic will be supplied, which is much more efficient than the classical double layer adsorption processes (Figure S13, Supporting Information).

To evaluate the capacitive performances of CDs/HPC and Free-HPC materials, three-electrode systems are employed using 3 M KOH, 4 M H_2SO_4, and 1 M Li_2SO_4 aqueous solutions as electrolytes, respectively. In **Figure 2**A–C, the nearly 90° turnings at the switching potentials in all cyclic voltammetry (CV) curves indicate that these samples respond very fast as capacitor materials. In the acidic electrolyte, NPOCD/HPC presents a pair of wide and symmetrical redox peaks due to the typical faradaic reactions.[30] However, in the alkaline and neutral conditions, there are no obvious peaks in CV curves, revealing that the capacitance is mainly from ions absorption. It is clear that with the similar surface area and pore volume, NPOCD/HPC shows much higher specific capacitances than Free-HPC because of its electron-rich regions. More importantly, due to the improved cations adsorption, NPOCD/HPC shows outstanding specific capacitances in various types of electrolytes, which is never dependent on pseudocapacitive reactions. The electrochemical performances of these samples are also investigated by galvanostatic charge–discharge (GCD) tests. As presented in Figure 2D–F, typical triangular shapes of these GCD curves are seen without any obvious ohmic drop. In the alkaline, acidic and neutral electrolytes, the optimal capacitances of NPOCD/HPC even reach 468, 510, and 438 F g^{-1}, respectively, meaning a dramatic increment of up to 70% over that of Free-HPC (Table S4, Supporting Information). In accordance with the CV tests, the capacitance increment is ascribed to the surficial reactions which are improved by the electron-rich regions. In comparison with other carbon materials in the literature, like mesoporous carbon, graphene based carbon, biomass based carbon, and so on (Table S5, Supporting Information), the present CDs/HPC materials show their superior merits in many aspects. Electrochemical impedance spectroscopy (EIS) is applied for further research on different samples (Figure 2G and Figure S16, Supporting Information). It is well known that a steeper linear curve in low frequency regions correspond to the ideal capacitances and semi-circles in high frequency region suggest the internal/surface resistance. Table S6 in the Supporting Information shows that CDs/HPC materials have lower interface resistances than Free-HPC. In addition, the operating frequency (f_0, the frequency at the half of the maximum capacitance value) and the characteristic relaxation time (τ_o) are the most critical quantitative indicators of how fast the materials can be charged–discharged reversibly.[35] In Table S6 in the Supporting Information, f_0 of the optimal sample NPOCD/HPC is just 0.55 Hz, much higher than Free-HPC (0.09 Hz). Therefore, CDs incorporation not only reduces the interface resistance of HPC, but also enhances the conductive stability of the electrode at high scan rates. Since the large electron-rich regions of NPOCD/HPC can accelerate cations transfer between the solutions and the interfaces, NPOCD/HPC shows a fast adsorption kinetics with a retention rate over 80% at high current densities (Figure 2H), which is obviously better than Free-HPC. To interpret the effects of mass loading, Figure 2I and Figure S17 in the Supporting Information shows that mass loading of NPOCD/HPC is increased by 10 times, the retention rates of specific

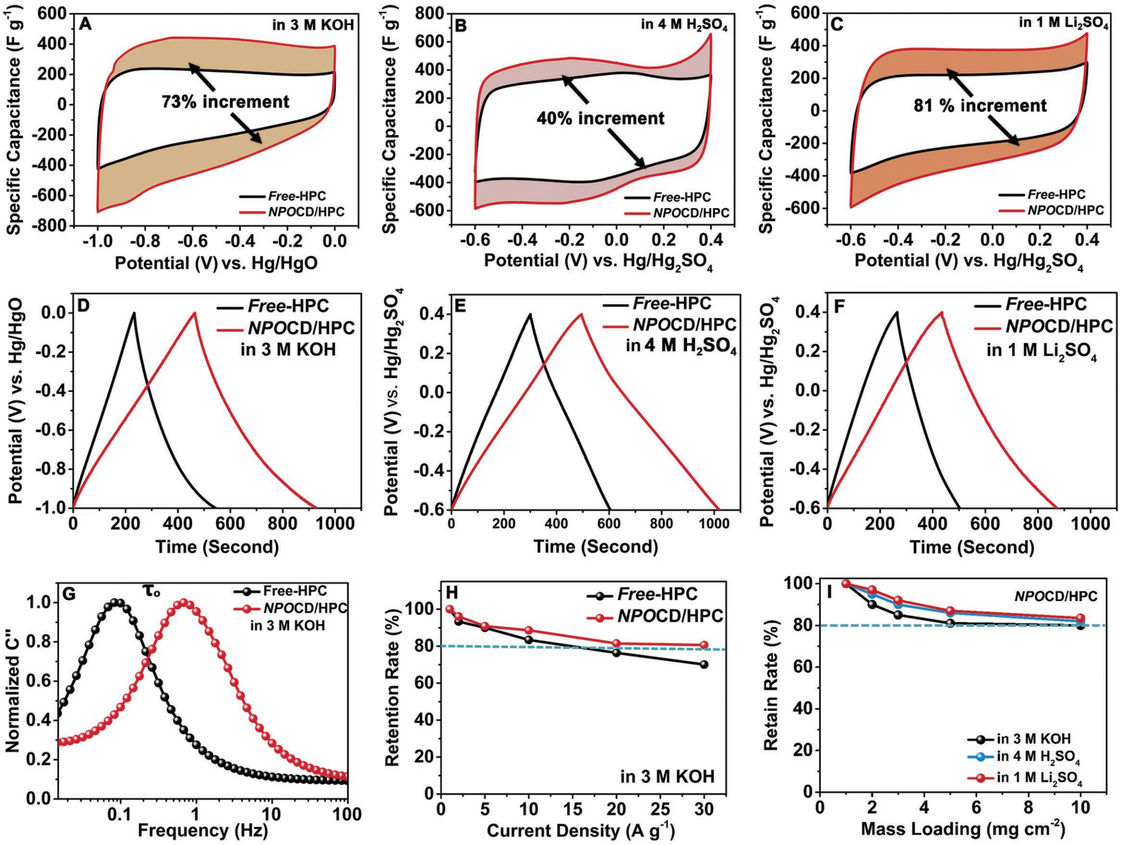

Figure 2. Electrochemical performances of NPOCD/HPC and Free-HPC in a three-electrode system. A–C) CV curves at a scan rate of 10 mV s^{-1} in alkaline (A), acidic (B), and neutral aqueous (C) solutions. D–F) GCD curves at current density of 1 A g^{-1} in the above three different aqueous solutions, respectively. G) The normalized imaginary parts of samples' capacitances versus frequency, which are derived from Nyquist plots (3 M KOH). H) The corresponding retention rates of Free-HPC and NPOCD/HPC. I) Retention rates of specific capacitance versus mass loading in different electrolytes.

capacitance are still above 80% in different electrolytes, which are superior to many similar carbon materials.[25,36,37]

For practical applications, a series of hybrid supercapacitors are fabricated by $Ni(OH)_2$, PbO_2 nanorods, and $LiMn_2O_4$ as the positive electrode materials (related GCD curves are shown in Figure S19 in the Supporting Information), and the optimal NPOCD/HPC as the negative electrode material, respectively. Although alkaline electrolyte has a lower hydrogen evolution potential, GCD curves of NPOCD/HPC//$Ni(OH)_2$ hybrid device (**Figure 3**A) still show an efficient and stable charge–discharge process because of the excellent reversibility and fast interface charge transfer of NPOCD/HPC. The mass ratio of positive/negative electrodes can be decreased to 1.6 by employing the optimal negative electrode material. As a result, the specific capacity of such hybrid device can reach 97 mA h g^{-1} (351 C g^{-1}) at 1 A g^{-1}, and the corresponding energy density can reach 90.1 W h kg^{-1} (based on total weight, Figure 3B). More importantly, the characteristics of high power density (10 530 W kg^{-1}) can still be finely retained at a pretty remarkable energy density of 60.8 W h kg^{-1}. Such performances are superior over many other $Ni(OH)_2$ related hybrid capacitors in the literature (Table S7, Supporting Information), including AC//β-$Ni(OH)_2$/MWCNTs, polyaniline–RGO//$Co_xNi_{1-x}(OH)_2$–RGO, graphene hydrogel//NiOOH nanosheets–graphene hydrogel, and nano FeOOH//Co–Ni double hydroxides.[38–41]

Further applications of the optimal negative electrode material are expanded in a more acidic electrolyte with the traditional PbO_2 positive electrode, and a neutral electrolyte with Li_2MnO_4 positive electrode, respectively (Figure 3C,E). Both systems exhibit a wide working voltage of 1.8 V and the symmetric GCD curves, indicating that our negative electrode material is compatible with various pH conditions. In addition, the energy density of hybrid supercapacitor exceeds 77 and 62 W h kg^{-1} in the acidic and the neutral conditions, respectively (Figure 3D,F), which are several times higher than those hybrid supercapacitors employing commercial AC, and biomass based carbon and nitrogen doped graphene as negative electrodes. Therefore, our CDs–hydrogel derived carbon material has not only a strong energy storage capability, but also a good compatibility with aqueous electrolytes in a wide range of pH values (Tables S7–S9, Supporting Information).

Cycling stability is an intrinsic advantage of carbon electrodes. Our hybrid supercapacitors exhibit 100% and 96% retention in 3 M KOH and 1 M Li_2SO_4 solutions at 10 A g^{-1} for 5000 cycles, respectively. Although the stability of conventional PbO_2 electrode is not ideal, the hybrid supercapacitor composited of NPOCD/HPC and PbO_2 nanorods process a retention over 91%. All these results are remarkably better than those of polymer or graphene based hybrid supercapacitors (Tables S7–S9, Supporting Information). In addition, at different mass

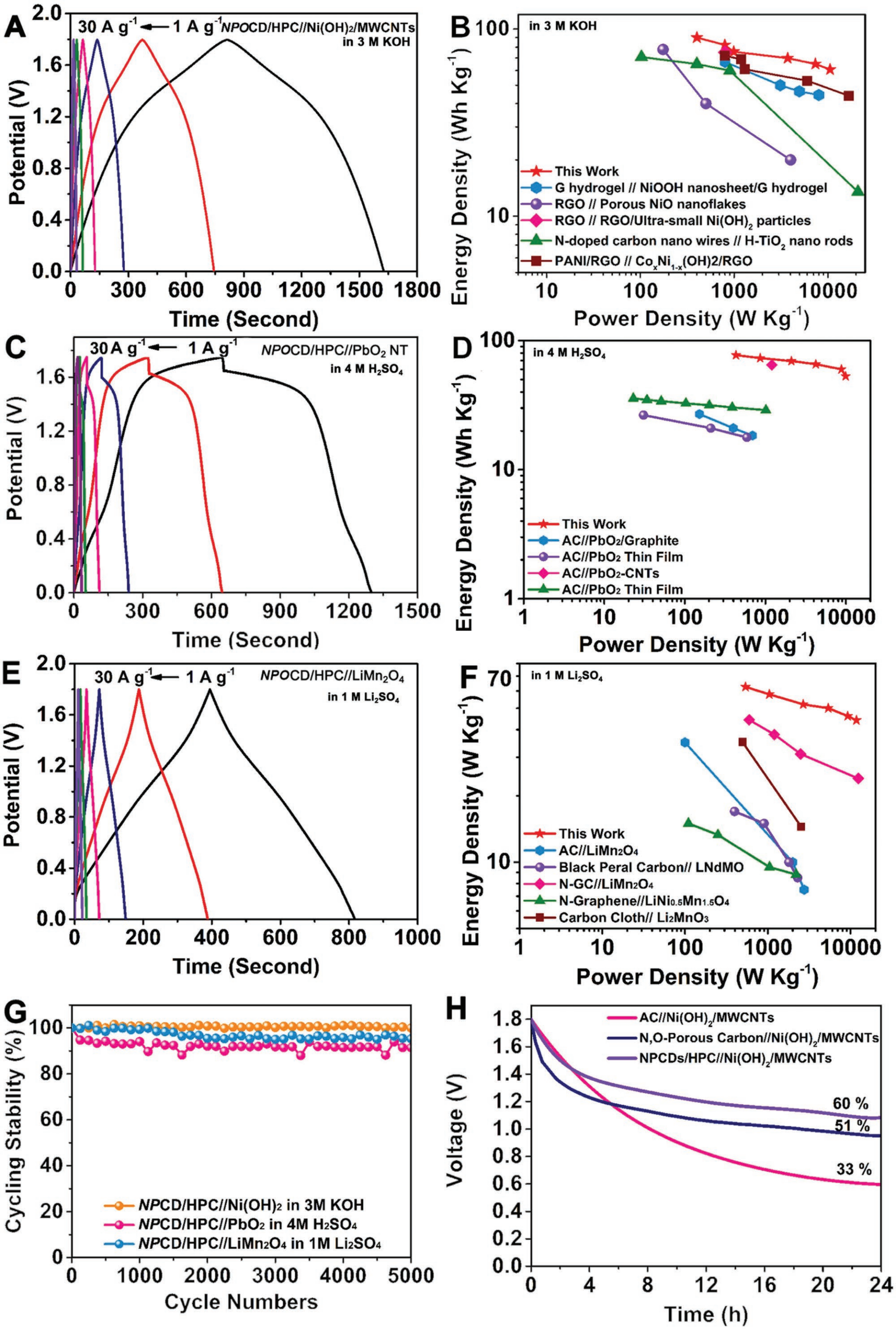

Figure 3. Electrochemical performances of the optimal hybrid supercapacitors in different electrolytes. A,C,E) GCD curves at different current densities in alkaline (A), acidic (C), and natural aqueous (E) solutions. B,D,F) Ragone plots (based on total weight of positive and negative electrodes) of the above devices in this work and other Ni(OH)$_2$/NiO, PbO$_2$, LiMn$_2$O$_4$ based hybrid supercapacitors in the literature, respectively (Tables S7–S9, Supporting Information). G) Cycling stability of hybrid supercapacitor in different electrolytes at current densities of 10 A g^{-1}. H) Self-discharge curves of hybrid supercapacitors with different negative electrodes.

loading (1–10 mg cm^{-2}, based on negative electrode materials, Figure S20, Supporting Information), energy densities and power densities of different hybrid devices also show high retention rates over 70%.

Finally, it is well known that self-discharge is an ineluctable problem for supercapacitors. In the present research, our hybrid device is precharged to 1.8 V immediately, and then its self-discharging is detected within 24 h (Figure 3H). This

© 2018 WILEY-VCH Verlag GmbH & Co. KGaA, Weinheim

device exhibits an obvious voltage drop of 0.25 V at the initial 4 h, and a slow voltage drop of 0.37 V in the next period of 20 h. For comparison, another hybrid supercapacitor using poly-Schiff base as the negative electrode material precursor, N, O-doped porous carbon//$Ni(OH)_2$/MWCNTs, shows a similar curve, but its voltage retention is only 51% after 24 h of self-discharging. When the commercial AC produced from coconut husks is used as the negative electrode material instead, the open voltage potential of this device declines continuously and the final retention rate is nearly 30% after 24 h. The advantage of our hybrid supercapacitor in self-discharging can be ascribed to the surface state constructed by CDs, which has numerous negative electric fields so as to restrain desorption of cations effectively (Figure S21, Supporting Information).

In summary, the cheap CDs–hydrogel derived carbon as a novel negative electrode material for hybrid supercapacitors, has outstanding advantages in energy density, power density, and cycling life, and also overcomes the common shortcomings of carbon negative electrode, like self-discharge, instability in acidic or alkaline electrolytes, and mismatch with different cations or positive electrode materials (Table S10 and Figure S22, Supporting Information).[8,42–45] All these merits are based on the outstanding properties of CDs which include controllable compositions, adjustable surface groups, good wettability, large surface areas, etc. The perfect combination between CDs and hydrogel frameworks make the surface states of carbon materials fit to be predesigned and adjusted until the practical demands are satisfied.

Supporting Information

Supporting Information is available from the Wiley Online Library or from the author.

Acknowledgements

This work was financially supported by the National Natural Science Foundation of China (Grant 21771039, 21622303), the Shanghai Science and Technology Committee (No. 16DZ2270100), and National Key Research and Development Plan (2016YFA0203302).

Conflict of Interest

The authors declare no conflict of interest.

Keywords

carbon dots, hierarchical porous carbons, hybrid supercapacitors, hydrogels, surface states

Received: September 25, 2018
Revised: November 12, 2018
Published online: December 9, 2018

---

[1] C. Zhu, P. Yang, D. Chao, X. Wang, X. Zhang, S. Chen, B. K. Tay, H. Huang, H. Zhang, W. Mai, H. J. Fan, *Adv. Mater.* **2015**, *27*, 4566.
[2] W. He, Z. Liang, K. Ji, Q. Sun, T. Zhai, X. Xu, *Nano Res.* **2018**, *11*, 1415.
[3] W. Zuo, C. Xie, P. Xu, Y. Li, J. Liu, *Adv. Mater.* **2017**, *29*, 1703463.
[4] P. Zhang, B. Y. Guan, L. Yu, X. W. D. Lou, *Angew. Chem., Int. Ed.* **2017**, *56*, 7141.
[5] Y. Huang, Y. Zeng, M. Yu, P. Liu, Y. Tong, F. Cheng, X. Lu, *Small Methods* **2018**, *2*, 1700230.
[6] H. Pang, X. Li, Q. Zhao, H. Xue, W.-Y. Lai, Z. Hu, W. Huang, *Nano Energy* **2017**, *35*, 138.
[7] N. Jabeen, A. Hussain, Q. Xia, S. Sun, J. Zhu, H. Xia, *Adv. Mater.* **2017**, *29*, 1700804.
[8] F. Wang, S. Xiao, Y. Hou, C. Hu, L. Liu, Y. Wu, *RSC Adv.* **2013**, *3*, 13059.
[9] J. Yan, Z. Fan, W. Sun, G. Ning, T. Wei, Q. Zhang, R. Zhang, L. Zhi, F. Wei, *Adv. Funct. Mater.* **2012**, *22*, 2632.
[10] Q. Qu, P. Zhang, B. Wang, Y. Chen, S. Tian, Y. Wu, R. Holze, *J. Phys. Chem. C* **2009**, *113*, 14020.
[11] P. Shang, J. Zhang, W. Tang, Q. Xu, S. Guo, *Adv. Funct. Mater.* **2016**, *26*, 7766.
[12] X. Yang, F. Qu, H. Niu, Q. Wang, J. Yan, Z. Fan, *Electrochim. Acta* **2015**, *180*, 287.
[13] J. Ni, H. Wang, Y. Qu, L. Gao, *Phys. Scr.* **2013**, *87*, 045802.
[14] N. Mahmood, C. Zhang, H. Yin, Y. Hou, *J. Mater. Chem. A* **2014**, *2*, 15.
[15] K. A. Owusu, L. Qu, J. Li, Z. Wang, K. Zhao, C. Yang, K. M. Hercule, C. Lin, C. Shi, Q. Wei, L. Zhou, L. Mai, *Nat. Commun.* **2017**, *8*, 14264.
[16] J. Wang, Y. Xu, B. Ding, Z. Chang, X. Zhang, Y. Yamauchi, K. C. Wu, *Angew. Chem., Int. Ed.* **2018**, *57*, 2894.
[17] W. Zuo, R. Li, C. Zhou, Y. Li, J. Xia, J. Liu, *Adv. Sci.* **2017**, *4*, 1600539.
[18] N. Choudhary, C. Li, J. Moore, N. Nagaiah, L. Zhai, Y. Jung, J. Thomas, *Adv. Mater.* **2017**, *29*, 1605336.
[19] H. Li, Y. Tao, X. Zheng, J. Luo, F. Kang, H.-M. Cheng, Q.-H. Yang, *Energy Environ. Sci.* **2016**, *9*, 3135.
[20] J. Li, X. Huang, L. Cui, N. Chen, L. Qu, *Prog. Nat. Sci.: Mater. Int.* **2016**, *26*, 212.
[21] D.-C. Guo, J. Mi, G.-P. Hao, W. Dong, G. Xiong, W.-C. Li, A.-H. Lu, *Energy Environ. Sci.* **2013**, *6*, 652.
[22] Q. Xue, H. Gan, Y. Huang, M. Zhu, Z. Pei, H. Li, S. Deng, F. Liu, C. Zhi, *Adv. Energy Mater.* **2018**, *8*, 1703117.
[23] L. Hu, C. Shi, K. Guo, T. Zhai, H. Li, Y. Wang, *Angew. Chem., Int. Ed.* **2018**, *57*, 8214.
[24] Y. Zhu, Z. Wu, M. Jing, H. Hou, Y. Yang, Y. Zhang, X. Yang, W. Song, X. Jia, X. Ji, *J. Mater. Chem. A* **2015**, *3*, 866.
[25] J.-S. Wei, J. Chen, H. Ding, P. Zhang, Y.-G. Wang, H.-M. Xiong, *J. Power Sources* **2017**, *364*, 465.
[26] X. Wei, X. Jiang, J. Wei, S. Gao, *Chem. Mater.* **2016**, *28*, 445.
[27] X. Wei, Y. Li, S. Gao, *J. Mater. Chem. A* **2017**, *5*, 181.
[28] X. Wei, H. Zou, S. Gao, *Carbon* **2017**, *123*, 471.
[29] X. Wei, S. Wan, S. Gao, *Nano Energy* **2016**, *28*, 206.
[30] J. S. Wei, H. Ding, Y. G. Wang, H. M. Xiong, *ACS Appl. Mater. Interfaces* **2015**, *7*, 5811.
[31] J. Ni, S. Fu, C. Wu, Y. Zhao, J. Maier, Y. Yu, L. Li, *Adv. Energy Mater.* **2016**, *6*, 1502568.
[32] G. Kresse, J. Hafner, *Phys. Rev. B* **1993**, *47*, 558.
[33] J. P. Perdew, K. Burke, M. Ernzerhof, *Phys. Rev. Lett.* **1996**, *77*, 3865.
[34] G. Kresse, D. Joubert, *Phys. Rev. B* **1999**, *59*, 1758.
[35] L. Wang, T. Wei, L. Sheng, L. Jiang, X. Wu, Q. Zhou, B. Yuan, J. Yue, Z. Liu, Z. Fan, *Nano Energy* **2016**, *30*, 84.
[36] C. Xu, Z. Li, C. Yang, P. Zou, B. Xie, Z. Lin, Z. Zhang, B. Li, F. Kang, C.-P. Wong, *Adv. Mater.* **2016**, *28*, 4105.
[37] M. D. Stoller, R. S. Ruoff, *Energy Environ. Sci.* **2010**, *3*, 1294.
[38] K. Chaitra, R. T. Vinny, P. Sivaraman, N. Reddy, C. Hu, K. Venkatesh, C. S. Vivek, N. Nagaraju, N. Kathyayini, *J. Energy Chem.* **2017**, *26*, 56.
[39] R. Wang, C. Xu, J.-M. Lee, *Nano Energy* **2016**, *19*, 210.

© 2018 WILEY-VCH Verlag GmbH & Co. KGaA, Weinheim

[40] B. Zhao, D. Chen, X. Xiong, B. Song, R. Hu, Q. Zhang, B. H. Rainwater, G. H. Waller, D. Zhen, Y. Ding, Y. Chen, C. Qu, D. Dang, C.-P. Wong, M. Liu, *Energy Storage Mater.* **2017**, *7*, 32.
[41] J. Chen, J. Xu, S. Zhou, N. Zhao, C.-P. Wong, *Nano Energy* **2016**, *21*, 145.
[42] A. Eftekhari, L. Li, Y. Yang, *J. Power Sources* **2017**, *347*, 86.
[43] Y. Zhang, S. Yu, G. Lou, Y. Shen, H. Chen, Z. Shen, S. Zhao, J. Zhang, S. Chai, Q. Zou, *J. Mater. Sci.* **2017**, *52*, 11201.
[44] Z. Lei, J. Zhang, L. L. Zhang, N. A. Kumar, X. S. Zhao, *Energy Environ. Sci.* **2016**, *9*, 1891.
[45] K. Wang, X. Zhang, C. Li, X. Sun, Q. Meng, Y. Ma, Z. Wei, *Adv. Mater.* **2015**, *27*, 7451.

© 2018 WILEY-VCH Verlag GmbH & Co. KGaA, Weinheim